Light Metals 2013 *Edited by: Barry Sadler*
TMS (The Minerals, Metals & Materials Society), 2013

A FULLY COUPLED THERMAL-ELECTRICAL-MECHANICAL TRANSIENT FEA MODEL FOR A 3D ANODE ASSEMBLY

D.R. Gunasegaram, D. Molenaar
Commonwealth Scientific and Industrial Research Organisation (CSIRO)
Private Bag 33, Clayton VIC 3169 (MELBOURNE) AUSTRALIA.

Keywords: Finite Element Analysis, Finite Element Method, Contact Resistance, Stub to Carbon Voltage Drop

Abstract

A fully coupled thermal-electrical-mechanical (TEM) transient model that simulates the rodding and cell operation phases of aluminum smelting in Hall–Héroult cells is presented and discussed. This 3D model of an anode assembly was developed using the commercial finite element analysis code Abaqus, and incorporates (i) temperature-dependent material properties as well as (ii) temperature- and pressure- dependent electrical contact conductance at the anode-thimble interface. The air gap between the anode and thimble is also taken into account through the predictions of (a) its formation during the rodding step, (b) its modification as the anode slides down under gravity on the flutes of the thimble during installation and (c) its partial closure as the components heat up and expand during cell operation. The predictions of the model are found to compare well with known plant measurements of temperatures and voltages for similar systems.

Introduction

It is well known that opportunities for significant energy savings exist in the electrical connections and in particular the stub-to-carbon (STC) connection of pre-baked anode assemblies used in Hall–Héroult cells [1-6]. Given that smelting of metals is highly energy intensive and is performed on a large scale, any small improvement made in the design of anode assemblies is likely to translate into a large saving in operating costs and, potentially, to a reduction in greenhouse gas emissions. For instance, for a country such as Australia where the consumption of 13% of all electricity generated is accounted for by the aluminum smelting industry [7], the benefits are expected to be substantial.

Recognizing the potential for improved design, several workers [e.g. 1-6] have modeled aspects relating to electrical connections for gaining deeper insights into factors affecting energy efficiency. Since numerical techniques are generally better suited to tackling complex real-world problems involving highly nonlinear physics, such methods have found favor over analytical techniques. In particular, finite element analysis (FEA) has been used as a modeling tool in the smelting industry since the 1980s.

Literature Review

Literature in the area was reviewed in recent years by Ding et al. [2], Beier et al [3] and Fortin et al [4]. Their reviews highlighted a need for modeling the operation of the anode assembly more realistically and in greater depth towards achieving significant improvements in performance. In collaboration with CSIRO, Ding et al [2] modeled the rodding and cell operation processes using a sequence of simulations using the commercial code Abaqus/Standard (version 6.10). Their model incorporated temperature- and pressure- dependent electrical contact resistance (ECR) at the anode-thimble interface (ATI) and temperature-dependent material properties. A major advancement attributable to their work was the calculation of the air gap at the ATI using a numerical solution rather than the more prevalent analytical approach. However, in simulating the gap formation, the workers first carried out an uncoupled heat transfer analysis using a constant heat transfer coefficient at the ATI and input the resulting temperature histories into a thermal-mechanical (TM) model. This approach excluded the influence of the expanding width of the evolving gap at the ATI in reducing the heat transfer rates at this interface, as would have happened in reality as solidification progressed. This lack of full two-way coupling between the thermal and mechanical physics therefore limited the predictions of the gap width in their work. Again, to calculate the gap widths during cell operation where parts heat up from the start-up stage, they first carried out a thermal-electrical (TE) simulation with a constant ECR and input the resulting temperature history into a TM model for cell operation. Once again, since Joule heating was not accounted for, the contribution of the electrical physics to thermal physics was not considered. In addition, since the mechanical and electrical physics were not coupled, the influence of the reducing gap at the ATI on ECR was not considered. From the TM run for cell operation, pressure at the ATI was obtained as a function of time. That pressure history was then input into a subroutine that determined ECR as a function of pressure and temperature in the final run, a TE simulation of the cell operation process. This last simulation output temperature and voltage profiles among other quantities. Ding et al used a similar approach in a subsequent work aimed at estimating the voltage losses attributed to stub tip deterioration in anode assemblies [8]. Beier et al [3] also investigated the impacts of stub deterioration in addition to that of yoke stiffness on the anode connection and hence on the performance of the anode assembly. They used the commercial code Ansys for meshing and, after some pre-processing with an in-house Laval University code FEsh++, they solved the steady state thermal-electrical-mechanical (TEM) cell operation problem also using FEsh++. However, the air gap was calculated analytically. The same software codes were used by Fortin et al [4] who also calculated the air gap analytically in their more comprehensive work. Their fully coupled TEM model for cell operation was used to iteratively obtain steady state solutions. The strategy was to first obtain convergence for the TE problem which included Joule heating capability, and to then solve the TM problem. Once convergence was obtained for the TM solution, a check was made as to whether the TE and/or TM solutions had changed considerably since the previous global iteration. The iterations were continued until no appreciable differences in solutions were obtained between subsequent iterations. Dupuis [5] used Ansys for his works on anodes and cathodes. However,

unlike Beier et al [3] and Fortin et al [4] who incorporated the air gap at room temperature in their CAD solid models, Dupuis [5] used varying reference temperatures (e.g. solidus temperature for cast iron and the average temperature during solidification for the anode and stubs) for thermal expansion in order to generate a value for the gap during his computations. Dupuis [5] also solved the steady state cell operation problem.

In summary, with the exception of the work of Ding et al [2,8], no worker appears to have attempted to develop a transient model for cell operation that would provide histories of variables such as temperature and voltages from start-up to half-rota and beyond. Also, apart from the model of Ding et al [2,8], no other work appears to calculate the size of the air gap by modeling the solidification process of the thimble. Finally, to the best of the authors' knowledge, no published work exists where a genuinely fully coupled TEM treatment is applied to a single transient model that covers both the rodding process as well as the subsequent cell operation process.

Aim and Modeling Strategy

As explained in detail by Fortin et al [4], the cell operation process involves two-way couplings between all physics involved: thermal, electrical and mechanical. The use of Abaqus/Standard version 6.11 in the current work enabled the use of fully coupled thermal-electrical-structural elements Q3D8 and Q3D4 which allowed for all the required couplings – making the simulations significantly more realistic. Each such element had degrees of freedoms related to displacement, temperature and voltage.

The aim of the work was, therefore, to develop a 3-dimensional transient continuum scale model that would simulate: (a) the rodding process employing fully coupled TM physics which would predict thimble geometry allowing for the creation of an air gap around the thimble during its solidification; (b) the sliding of the anode under gravity on the thimble flutes when the aluminum rod was lifted up for clamping onto the anode beam – modifying the gap widths in the process, and finally (c) the cell operation process to half rota employing TEM physics. It was intended that Joule heating be included.

Before the analysis, the entire geometry, including the cover (crust), was solid modeled as an assembly of parts - without any gaps between the thimbles and the anode. Once pre-processing was completed, the solution scheme was prescribed as illustrated in Fig. 1. As the cover is not present during the rodding phase, its elements were deactivated before the rodding step and reactivated immediately after the rodding step. In order to ensure contact between the anode and the reactivated cover was not lost due to thermal expansion or contraction, the entire assembly was given sufficient time in the rodding step to cool down to 293 K (20 °C), the initial temperature of all parts, except the thimbles. The next step simulated anode descent which was followed by the final step, cell operation. SI units were used throughout.

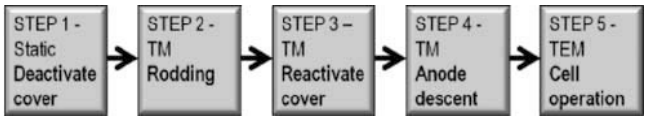

Figure 1. Modeling strategy used in the present work.

Abaqus/Standard assumes that electrical equilibrium is achieved instantaneously, thus neglecting transient electrical effects. This is acceptable at the continuum scale at which the present model was developed since electron motions occur at a time scale associated with much smaller length scales.

Description of the Model

Software and Hardware

Abaqus/Standard v6.11 was run on a single compute node, shared memory environment on CSIRO's High Performance Computing Centre with 12 processors. The direct solver was used with 12 domains with full integration for the Newton-Raphson solution scheme.

Geometry

The geometry (Fig. 2) comprised an assembly which included the aluminum rod, the transition joint, the yoke (crossbar), four stubs, welds, the anode (with half rota dimensions), four thimbles and cover. While it resembled assemblies used in commercial pre-baked anode technologies, the geometry was deliberately created to represent a generic design.

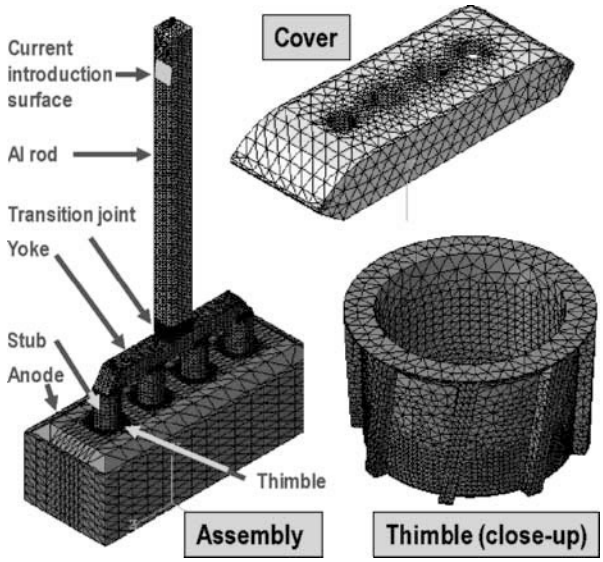

Figure 2. Geometry and mesh used for simulations. Colors depict various materials. The surface on which electrical current was introduced into the model is also shown.

Mesh statistics

Details of the mesh used are presented in Table I and shown in Fig. 2. Since tetrahedral elements lend themselves to convenient meshing of parts with complex geometry, those elements were used for all parts except the titanium layer of the transition joint. The latter was meshed with first order hexahedral elements since its small thickness (0.002 m) would not allow undistorted tetrahedrons to be used. The use of first order tetrahedron elements is justified for the first version of this model on the basis that (i) the elements were sufficiently refined (Fig. 2) in areas where large gradients were expected and (ii) their distortion was minimal during the simulations. Further justification of this decision will be presented later in the form of results which were comparable to plant measurements for similar systems.

Table I. Mesh statistics

Part	Number of Nodes	Element Type	Number of Elements	Typical Edge Length of Element (m) Fine/Coarse
Anode	22948	Q3D4	90144	0.005/0.120
Cover	2075	Q3D4	7703	0.20/0.110
Al rod etc.	25462	Q3D4	103084	0.001/0.040
		Q3D8*	7703	
Thimble 1	6600	Q3D4	25875	0.005/0.020
Thimble 2	6600	Q3D4	25875	0.005/0.020
Thimble 3	6600	Q3D4	25875	0.005/0.020
Thimble 4	6600	Q3D4	25875	0.005/0.020

* For the Titanium layer of the transition joint.

Material Properties

Materials designated for the parts are listed in Table II.

Table II. Material designations for parts

Part	Material
Anode	Baked anode carbon
Cover	50% solid bath + 50% alumina
Aluminum rod	Al6061
Aluminum weld	Al4043
Ti layer on joint	Commercial purity Ti
Yoke	SAE1020
Stubs	SAE1020
Steel weld	SAE1020
Thimbles	Grey cast iron

Temperature-dependent material properties obtained from the public domain were used for most materials. For the cover, which is a non-standard material, properties other than thermal conductivity were assumed to be the arithmetic averages of those for the cryolite bath and alumina. For the thimbles, custom data on thermal expansion coefficient was generated at CSIRO. All materials were treated as exhibiting elastic behavior.

Boundary Conditions

Thermal boundary conditions: Typical conduction and convection heat transfer coefficients (HTCs) were defined for calculating heat exchange between the solid bodies and their local ambient (see Table III). Radiation from the hot bath to the sides of the anode and the bottom of the cover was also modeled.

During the rodding simulation, all external boundaries were assumed to be exposed to an ambient temperature of 293 K (20 °C) and to exchange heat with the ambient in convection mode with HTC = 30 $Wm^{-2}K^{-1}$. HTCs between other interfaces were the same as those used for the cell operation step (Table III). The thimble nodes started at a temperature of 1673 K (1400 °C) whilst the rest of the components were at 293 K at the start of the casting step. At the end of the casting step (lasting 36,000 s or 10 h), all components had reached the ambient temperature. In the cell operation step, all parts started at the initial temperature of 293K and the transient run continued up to 172,000 s (= 47.7 h) by which time steady state had been reached. Note that in the plant there would be minor changes occurring past this stage in temperature profiles, and therefore in voltage profiles also due to temperature-dependent electrical resistivities, as the anode size continuously decreases owing to consumption.

Table III. Thermal boundary conditions for the cell operation step

Interface	HTC ($Wm^{-2}K^{-1}$) at [gap] (m)	Electrical Contact Conductance (S/m^2) at [gap] (m)
CONDUCTIVE		
Thimble-anode	10,000 [0.0] 0 [0.001]	Variable**
Thimble-stub	1,000 [0.0] 0 [0.002]	3E8 [0.0] 3E8 [0.0005] 3E8 [0.002]
Anode-stub	Insulating	Insulating
Boundaries involving cover	Insulating	Insulating
CONVECTIVE		
Top half of Al rod (exposed to ambient temperature of 373 K or 100 °C)*	20	
Middle part of the anode in the region that is above the cryolite bath but below the cover (exposed to an ambient temperature of 1173 K or 900 °C inside the steel shell)	20	
All other surfaces (exposed to an ambient temperature of 500 K or 227 °C inside the hood)	20	
RADIATIVE	View factor	
Surfaces exposed to the bath maintained at 1233 K or 960 °C (sides of the anode and bottom of the cover)	0.9	
PRESCRIBED TEMPERATURE All nodes on the bottom surface of the anode and those on the sides inside the immersed region were raised from 293 K (20 °C) at 0 s to 1233 K (960 °C) in 3600 s to account for the heating up due to contact with the bath.		

* Elevated temperature was used here to account for radiative effects from the hood beneath.

**Temperature- and pressure- dependent values from Molenaar et al [1] used in tabular form.

Mechanical boundary conditions: In the rodding step, the floor on which the anode rests was defined by restricting the vertical (y-direction, see Fig. 2) movements of all nodes at the bottom surface of the anode. To prevent rigid body motion (RBM) of the anode, two of those nodes at the centre of the anode were also fixed in the x and z directions. Both these boundary conditions were deactivated in the anode descent step where the anode has to slide under gravity. In the cover reactivation step, the nodes on the top surface of the aluminum rod were constrained from movement in all directions to prevent RBM of the assembly.

As far as contact was concerned, a penalty frictional formulation with a coefficient of friction of 0.2 was used with finite sliding in the tangential direction and hard pressure overclosure was assumed in the normal direction. However, the coefficient of friction was increased to 1.5 for the thimble-stub interface after the rodding step to prevent slippage, so as to account for the fact that the thimbles were firmly secured on to the stubs following solidification.

Electrical boundary conditions: In the cell operation step, which was the only step in which the electrical degrees of freedom were active, the nodes at the bottom of the anode were prescribed a zero voltage, designating that surface as the electrical ground. All nodes in the cover also were prescribed zero voltage to prevent current leakage into this electrically insulating part.

Loads

Only two loads were defined, the gravity load acting in the negative y direction from the rodding step onwards and the electrical current active only in the cell operation step. The current was introduced as a density on the surface shown in Fig. 2 corresponding to the overlap of the aluminum rod and the anode beam. The total current introduced thus was 14.8 kA (= 3.7 kA per stub). It was ramped from 0 A at 0 s of the cell operation step to its maximum value in 3600 s (1 h) to account for the phenomenon of the progressive dissolution of the electrically insulating bath freeze. Buoyancy effects of the bath on the anode were neglected.

Results and Discussion

Run times

The entire simulation comprising the five steps (Fig. 1) was completed in 32.50 h. CPU time used was 245.75 h, memory usage = 13.1 GB and virtual memory usage = 18.3 GB.

Positions of 'Virtual Probes'

Certain nodes on the anode, thimble and stub were selected as virtual probes and predicted histories of temperature, displacement and voltage were saved at these locations during the simulation. Positions of these nodes are shown in Fig. 3. These were located between an external thimble and the adjacent thimble, and on a horizontal plane roughly at the centre height of the thimbles and on the vertical symmetry plane of the anode.

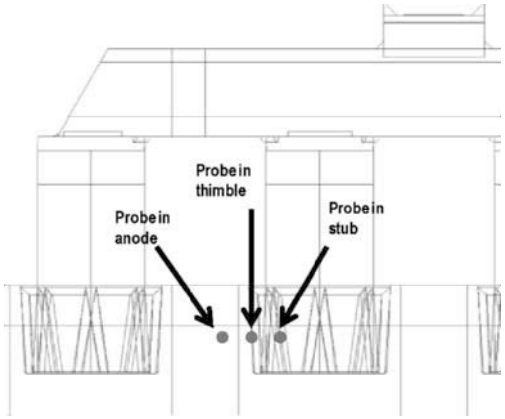

Figure 3. Positions of 'virtual probes'. Front view shown here in transparent style.

Temperature Profiles and History (Figs. 4-7)

Although solutions to temperature were generated in K, results (Figs. 4-7) are presented in °C to better align with industry practice. Temperature profiles in the rodding step during solidification are shown in Fig. 4 about 3 min after the pour and the grey cast iron cooling curve is shown in Fig. 5. The predicted temperature profiles during the steady state cell operation (Figs. 6-7) are consistent with measurements made at plants for similar systems [9]. These enhance the level of confidence in the temperature predictions of the model.

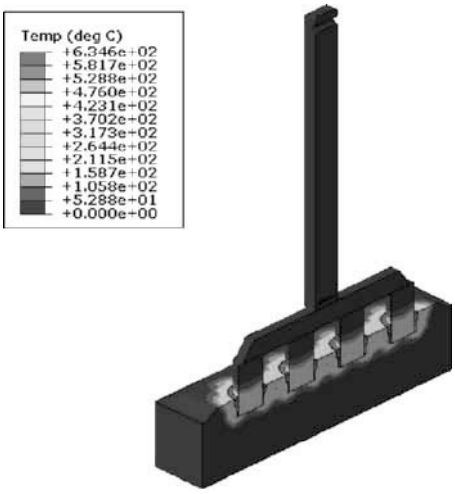

Figure 4. Temperature profile (°C) in the assembly during the rodding step about 180 s (3 min) after pouring the molten grey cast iron.

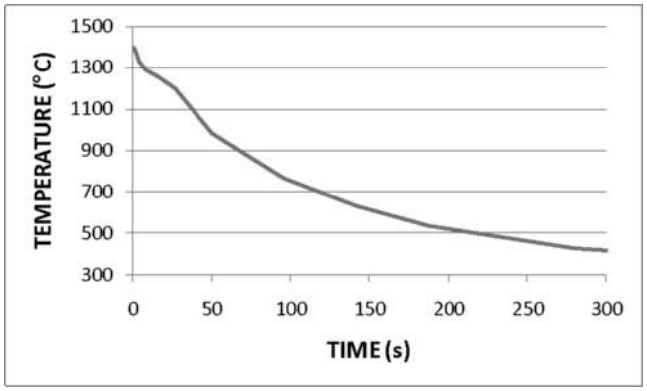

Figure 5. Temperature history (°C) in the thimble during the first 300 s (5 min) of the rodding step.

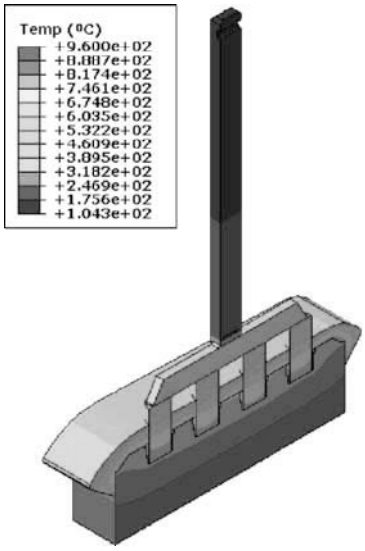

Figure 6. Temperature profile (°C) in the assembly at steady state in the cell operation step.

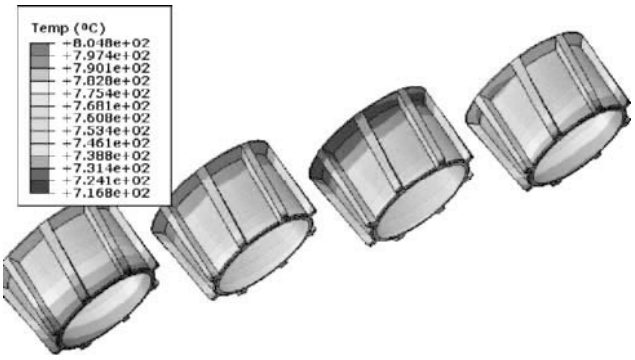

Figure 7. Temperature profile (°C) in the thimbles at steady state in the cell operation step.

Displacement Profiles and History (Figs 8-9)

The displacement calculations correctly predict that the gaps around the thimble castings at the end of the rodding step are non-uniform (Fig. 8) and that there is toe-in of the stubs into the anode as described by Fortin et al [4] (Fig. 9). Additionally, the anode was predicted to slide down relative to the thimble under gravity by about 0.7 mm during installation.

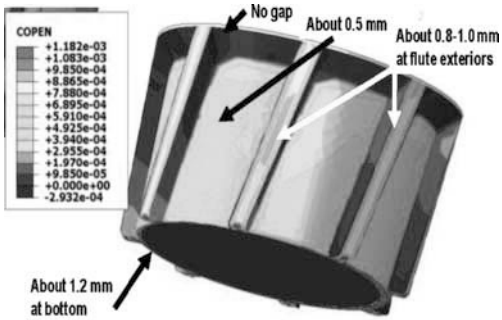

Figure 8. Gaps (m) around a thimble (2nd from left) at the end of the rodding step. The casting rests on the anode at the zones marked with black contours (no gap).

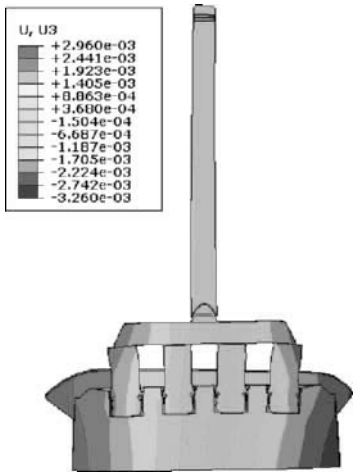

Figure 9. Displacement (m) in the horizontal direction during steady state cell operation highlighting the 'toe-in' effect. Magnification 50x.

Stresses and Strains (Figs. 10-11)

As indicated by captions to Figs. 10-11, the simulations provide estimates for quantities that are difficult to measure in practice, opening up possibilities for more informed designs. Unusually high stresses in Fig. 10 are due to the use of only elastic properties in the current model and may be addressed by the addition of plastic deformation in future models.

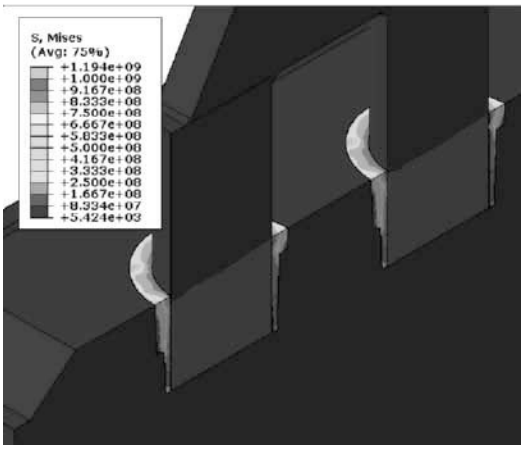

Figure 10. Maximum von Mises stresses (Pa) at the end of the rodding step, highlighting the contraction related stresses in the castings and stubs.

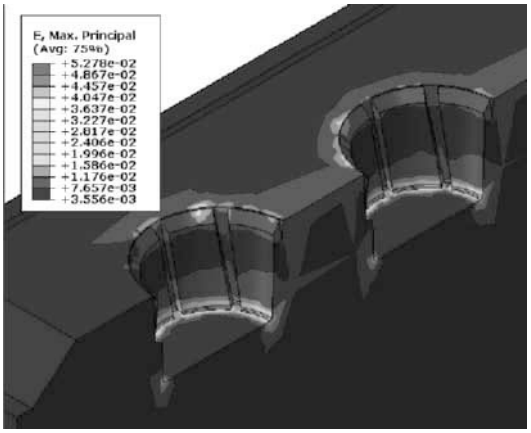

Figure 11. Maximum principal strains (-) on the anode during the steady state of the cell operation step, showing the impact of high contact pressures at the bottom of the stub holes.

Voltage Profiles and History (Figs. 12-14)

The 0.332 V voltage drop predicted in the assembly (Fig. 12) is in accordance with observations made in smelters (see also [4]). Likewise, the STC voltage drop (Fig. 13) of 0.110 V agrees well with the 0.120 V reported by Wilkening and Cóte [9]. The voltage history of the thimble (Fig. 14) shows that initially its voltage increases with current (keeping in mind the bottom of the anode is the electrical ground). However, as the differential expansion between the thimble and anode during heating results in better contact between these parts, there is a reduction in the STC voltage drop relating to the virtual probes shown in Fig. 3.

Electrical Current Density (ECD) Profile (Fig. 15)

As with the stresses and strains, ECD profiles (Fig. 15) provide an indication of a quantity that is not easily measured in the high temperature environment of a smelter, and thus is highly useful.

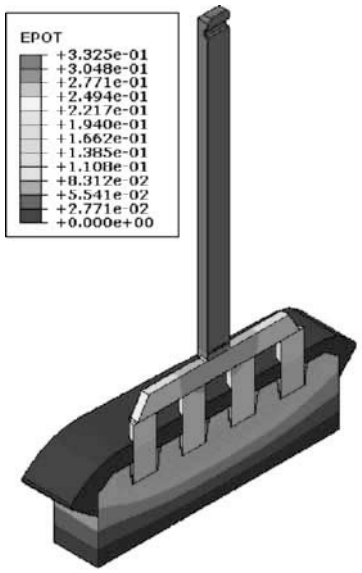

Figure 12. Voltage profiles (V) during the steady state cell operation. The total voltage drop is shown to be about 0.332 V, consistent with plant measurements [2].

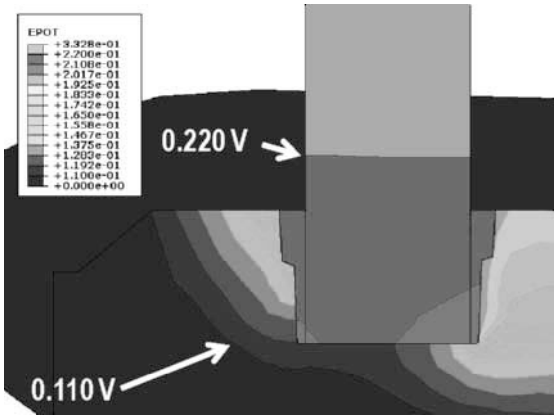

Figure 13. STC voltage drop (V) during the steady state cell operation. The figure of (0.220 – 0.110) = 0.110 V is consistent with 0.120 V measured [9] for a similar system.

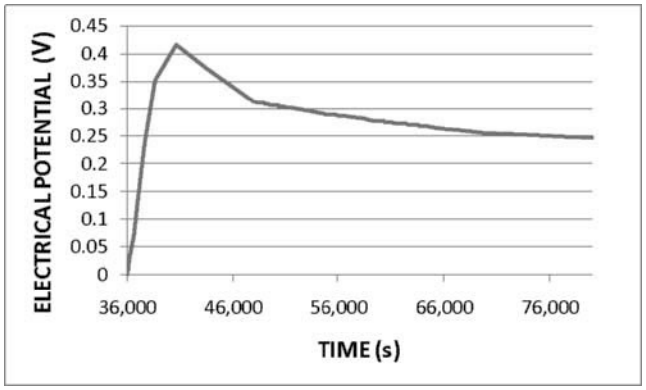

Figure 14. Voltage history of thimble during the cell operation step. Units are V for electrical potential and s for time starting at the beginning of the cell operation step.

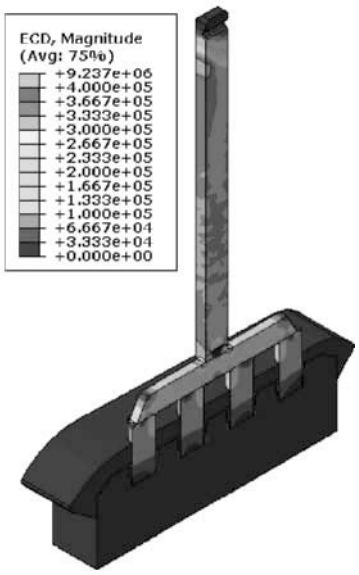

Figure 15. Electrical current density (Am^{-2}) profiles during the steady state cell operation.

Concluding Remarks

A fully coupled 3-dimensional transient thermal-electrical-mechanical finite element model that simulates the rodding and the subsequent operation phases of the anode assembly in Hall–Héroult cells was presented and discussed for the first time. Its predictions of temperatures, displacements and voltages were found to compare favorably with known plant measurements in systems similar to that considered here. It is intended that this model would be progressively refined with the use of more realistic inputs and hexahedral elements.

References

1. D. Molenaar, K. Ding and A. Kapoor, "Development of industrial benchmark finite element analysis model to study energy efficient electrical connections for primary aluminium smelters", *Light Metals 2011*, 985-990.

2. K. Ding, D. Molenaar and A. Kapoor, "Prediction of voltage loss on electrical connections for aluminium smelter reduction cells", *Procs. Of the Inst. Of Mech. Engrs., Part C, Journal of Mechanical Engineering Science*, (2011) 1-14.

3. S. Beier, J.J.J. Chen, H. Fortin and M. Fafard, "FEM analysis of the anode connection in aluminium reduction cells", *Light Metals 2011*, 979-984.

4. H. Fortin, N. Kandev and M. Fafard, "FEM analysis of voltage drop in the anode connector induced by steel stub diameter reduction", *Finite Elements in Analysis and Design*, 52 (2012), 71-82.

5. M. Dupuis, "Development and application of an Ansys based thermo-electro-mechanical collector bar slot design tool", *Light Metals 2011*, 519-524.

6. D. Richard, P. Goulet, O. Trempe, M. Dupuis and M. Fafard, "Challenges in stub hole optimisation of cast iron rodded anodes", *Light Metals 2009*, 1067-1072.

7. Anon., "Sustainability Report 2009", (Australian Aluminium Council Limited, Canberra, 2009).

8. K. Ding, D. Molenaar and A. Kapoor, "FE modeling of voltage loss during stub tip deterioration in anode assemblies", (Paper presented at the 10th Australasian Aluminium Smelting Technology Conference, Launceston, Australia, October 10-14, 2011).

9. S. Wilkening and J. Cóte, "Problems of the stub-anode connection", *Light Metals 2007*, 865-873.